Desalination and Water Treatment
www.deswater.com

doi: 10.5004/dwt.2023.29985

312 (2023) 234–246
November

Optimization of operational parameters in photocatalytic degradation of methylene blue using zeolitic imidazolate framework-11 nanostructure

Fateme Houshyar[a], Mohsen Mehdipour Ghazi[a,*], Narjes Keramati[b]

[a]*Department of Chemical, Petroleum and Gas Engineering, Semnan University, Semnan 35131-19111, Iran, emails: mohsenmehdipour@semnan.ac.ir (M. Mehdipour Ghazi), fatemehoushyar@semnan.ac.ir (F. Houshyar)*
[b]*Department of Nanotechnology, Faculty of New Sciences and Technologies, Semnan University, Semnan 35131-19111, Iran, email: narjeskeramati@semnan.ac.ir*

Received 8 November 2020; Accepted 17 September 2023

ABSTRACT

In this research, synthesis, characterization, and photocatalytic degradation of zeolitic imidazolate framework-11 was investigated. This framework was synthesized through a solvothermal method using the polar solvent, methanol. The characterization analysis included X-ray diffraction analysis, energy-dispersive X-ray spectroscopy, field emission scanning electron microscopy, Brunauer–Emmett–Teller, Fourier-transform infrared spectroscopy, and contact angle measurement; which have been discussed to characterize the as-synthesized nanostructure zeolitic imidazolate framework-11 (ZIF-11). As a result of diffuse reflectance spectroscopy analysis, ZIF-11 was recognized as photoactive with a band gap of 5 eV. The contact angle in the synthesized photocatalyst was 166° showing that it is hydrophobic. Evaluating the effect of operational factors including pH, photocatalyst dosage, and aeration pump flow rate in the photodegradation process was done by performing 22 experiments via Design-Expert software through the response surface method. The most and least effective parameters were identified as pH and aeration pump with contribution percentages of 33.82 and 2.57, respectively. A quadratic theoretical model with a *P*-value of less than 0.0001 for the photodegradation process was obtained. The optimal degradation percentage of methylene blue as organic waste, in minimum aeration pump level, pH equal to 10, and 0.2 g of the photocatalyst was observed to be 83.88% under UV light irradiation in 30 min. The value obtained for *R*-squared in this model was 0.9996, which would validate the accuracy and adequacy.

Keywords: Solvothermal; Photocatalyst; Methylene blue; Zeolitic imidazolate framework-11 (ZIF-11)

1. Introduction

Clean water scarcity is reported to be observed in arid regions, where over 100 million people live, in 2025 [1]. The hazardous components presented in industrial wastewater are categorized into various groups, including surfactants, detergents, greases, hydrocarbons, polyaromatic compounds, volatile organic compounds, pharmaceutical products, organic dyes, and heavy metal pollutants [2–4].

The textile industry is responsible for one of the greatest waste streams its main problem is consuming a vast majority of water that would be altered to thoroughly contaminated wastewater [5–8]. This industrial branch not only utilizes the highest amount of consumable water among other industries but also produces the greatest amount of waste consisting of synthetic organic compounds known as dyes [6,9]. Dyes could become a serious threat to the life of many different species [3,5,9]. An in-demand yet hazardous substance, methylene blue, which is widely used in textile production chains, can cause serious discomfort and irritation for human beings from eye burn to breathing difficulty and mental confusion [10]. Consequently, the necessity

* Corresponding author.

of discovering an efficient route to overcome this problem is a well-known fact [9,10].

Textile factories need to take advantage of special advanced water recovery utilities to close the water cycle for a sustainable waste treatment process. The most effective processes include membrane [11,12], adsorptive [13,14], biological [6,15,16], and more commonly used; advanced oxidation processes (AOPs) [17–19]. Considering the transforming or concentrating the pollutants into one phase, within membrane and adsorptive processes, biological and AOPs could be a perfect alternative for the complete removal of contaminants [3,6,12].

The mineralization could occur as a consequence of colliding a photon, having a sufficient amount of energy, with the surface of the photocatalyst. The cooperation will form electron holes in the valence band and thereafter reductive or oxidative transformations of organic wastes occur [20,21]. Substantial photocatalysts known as semiconductors (eg., TiO_2, ZnO, Fe_2O_3, CdS, Ag_2O, and ZnS) have extensively been applied for toxic and hazardous waste treatments [3,20]. The drawbacks of these materials include the corrosion of semiconductors in aqueous media and under light irradiation [3], immediate electron–hole pair separation, and limited adjustable structural behavior [22,23]. To address these disadvantages, metal–organic frameworks (MOFs) as newly applicable compounds, have recently been introduced [3,24]. Following considerations have emerged a brilliant notion about MOFs' application in photocatalytic activities. Firstly, some MOFs behave as a semiconductor, regarding the photoexcitation of metal ions or organic linkers. Secondly, the activated organic linker or the unsaturated metal clusters – consisting of these frameworks – could perfectly perform catalytic activities [25].

A significant and efficient subclass of MOFs is categorized as zeolitic imidazolate frameworks (ZIFs), which are structurally alike the zeolites as the name represents. This class of porous polymers could fit precisely in a position between MOFs and zeolites possessing the benefits of both materials [26]. Zeolitic supports enhance the photoactivity of the supported semiconductor by their internal electric field [27]. Due to the high adsorption capacity of zeolites, organic pollutant molecules would be brought to the surface of the photocatalyst, where hydroxyl and superoxide radicals exist [28]. Furthermore, the favorable thermal and chemical stability of these frameworks, more specifically ZIF-8 and ZIF-11, have attracted great scientific demand and funds for their usage in various applications [29]. The stability of the aforementioned ZIFs has been proved by not being decomposed in a 500°C heating environment and harsh ambiances such as boiling benzene, water, aqueous sodium hydroxide, and methanol. The outstanding resistance to hydrolysis in these two ZIFs could be best explained by the hydrophobic nature of surface structure and pores. This structural characteristic prevents ZnN_4 unit attack and framework dissolution in water [30].

ZIF-11 could be easily synthesized through a solvothermal route via different solvents; N,N-diethylformamide (DEF) [31,32], and methanol or ethanol [30]. Absorbance simulations of ZIF-11 have been studied for both hydrogen [33] and carbon dioxide [34]. Adsorption applications were also investigated for carbon dioxide [35,36] and polycyclic aromatic hydrocarbons [37]. ZIF-11 applicability in membrane processes exhibited cognitive performance for H_2 separation (applying the framework solely [38] and in mixed matrix membranes [39–41]) and ethylene diffusion [42]. ZIF-11 studies have not yet covered the efficient and bio-degradable method for organic waste treatment, which is its photocatalytic application.

The methylene blue degradation process was precisely studied using ZIF-8 under UV irradiation light (500 W), resulting in 82.3% removal in 120 min [43]. The degradation process was confirmed by the photoluminescence method through hydroxyl radical detection. The effect of initial dye concentration and pH value were also investigated. The most effective pH value was considered to be alkaline mediums for the increased OH radical formation based on the higher OH^- concentration. The other study investigated Rhodamine B removal using ZIF-67 as a photocatalyst to activate peroxymonosulfate (PMS). The dye degradation percentage was calculated as 90% in 60 min [44]. Other MOFs being analyzed are listed below: MOF-199 (99.0% removal of Basic Blue 41 in 180 min) [45], MIL-100 (99.2% removal of Basic Blue 41 in 180 min) [46], MIL-53(Fe) (complete removal of Malachite green in 40 min) [47].

One-factor-at-a-time (OFAT) experiments working on just one variable parameter while other factors are constant, is a method that is widely used in statistical measurements. Even though, by taking advantage of the Design of Expert (DOE) and more specifically response surface method several variable factors could be investigated simultaneously. Moreover, the effect of each parameter on the obtained result and the interaction between various factors in the DOE method would be achieved more precisely [48].

ZIF-11, as a highly stable and resistant zeolitic imidazolate framework was chosen to evaluate its photoactivity in dye degradation performance. This study first examined the photocatalytic applicability of ZIF-11 for the methylene blue degradation process. Secondly, it investigated the influential parameters in this process using RSM (response surface method) in Design-Expert software.

2. Experimental set-up

2.1. Materials

Reagents and chemicals in this study were used without any purification and purchased in analytical grade. Benzimidazole ($C_7H_6N_2$) was purchased from Sigma-Aldrich (USA). Zinc acetate dihydrate, hydrochloric acid 37%, sodium hydroxide, methylene blue, and acetone were supplied from Merck (Germany). Methanol, toluene, and ammonium hydroxide 30% were purchased from Dr. Mojallali's Industrial Chemical Complex Co., (Iran).

2.2. Preparation of ZIF-11

The crystals of ZIF-11 were successfully prepared according to the method reported by He et al. [49] with slight modification. The selection of the solvothermal method among other available synthesis routes was done because of the better solubility of heavy organic molecules, and acceleration of the nucleation process to rapidly initiate the complex formation [50]. Methanol was chosen for the synthesis

procedure because of its higher polarity compared with ethanol. 2.88 g benzimidazole was dissolved in 72 mL methanol under stirring at 4,000 rpm. Then 64 mL toluene and 18 mL Ammonium hydroxide were dropped into the above solution. After 10 min of stirring, 1.33 g zinc acetate was added, and the solution was stirred for 3 h at room temperature. After that, the suspension was filtered with filter paper and washed with methanol three times to ensure the complete removal of trapped toluene molecules. Then the filter paper containing wet crystals was located in an oven at 70°C overnight to achieve the pure ZIF-11 phase. The synthesis procedure is presented in Fig. 1.

2.3. Characterization

Powder X-ray diffraction (PXRD) analysis has been performed on an X-ray diffractometer (XRD, D8/Bruker, Germany). Energy-dispersive X-ray spectroscopy (EDX) and field emission scanning electron microscopy (FESEM, TESCAN MIRA3 XMU, Czech Republic) were used to investigate the morphology and molecular composition. Brunauer–Emmett–Teller (BET) surface area and N_2 adsorption–desorption isotherms were also examined by a BELSORP Max Micropore and Chemisorption Analyzer (Japan). The structural bindings were observed through a Fourier-transform infrared spectroscopy test (FTIR, Shimadzu, Japan). The powder photocatalytic activity has been measured by a diffuse reflectance spectroscopy analysis (DRS, Avantes, AvaSpec-2048-TEC, Netherlands). To investigate the hydrophobicity of the material CA-ES.10, Fanavary-Ezdiad-Bardasht-Fars contact angle measuring instrument, Iran was applied. Measuring the photodegradation percentage was done by a T80plus, PG Instrument, England.

2.4. Photocatalytic degradation experiments

The photocatalytic degradation process was performed in a 300 mL photocatalytic reactor. The reactor has a circulation system for temperature adjustment using a water pump, an aeration pump to supply the oxygen demanded for photoactivity, and four places for light sources. Four 6-W Philips UV lamps had been utilized to provide the light. In a typical reaction, the photocatalyst powder was added to 100 mL water and dispersed in water by placing it on a magnet stirrer at 8,000 rpm for 90 min. Methylene blue (10 ppm) was also prepared to be added to the photoreactor. The reactor was then placed on a magnet stirrer at 2,000 rpm and with the aeration pump ON, in the dark for 30 min to ensure the occurrence of the adsorption–desorption equilibrium. The photoreactor schematic is presented in Fig. 2.

The UV lamps were then lightened to trigger the photoactivation of the photocatalyst. In each 3 min during the photocatalytic reaction, 10 mL of solution was collected and centrifuged at 5,500 rpm. The degradation amount of dye was then measured by a UV-visible spectrophotometer at 664 nm. The 664 nm wavelength which has been chosen to study the methylene blue (MB) degradation trend, is in good match with the previous studies. Since maximum UV-Vis absorption of MB monomers, oligomers (dimmers and trimmers) appeared at 668 and 624 nm, and 606 and 565 nm, respectively. Thus, because of easily broken rapidly broken MB monomers in comparison to its oligomers in which longer degradation time is needed, 664 nm has been selected for investigations of MB degradation [51]. The degradation percentage was calculated according to the Eq. (1):

$$\text{Degradation}\,\% = \frac{C_0 - C_f}{C_0} \times 100 \tag{1}$$

Fig. 1. ZIF-11 synthesis procedure.

where C_0 and C_f represent the MB concentration at the beginning and the end of the reaction.

In this study, a new parameter known as R is introduced, which would be replaced with degradation percentage. R would be defined as Eq. (2), and it will be the main result in the following steps:

$$R = \frac{\text{Degradation}\%}{\text{photocatalyst}(\text{gr}) \times \text{time}(\text{min})} \quad (2)$$

As observed, the higher amount of R leads to better degradation results. Higher R indicates lower usage of photocatalysts and less time, which both account for ecological benefits in various industries.

2.5. Design of experiments

Three operational parameters (pH and photocatalyst dosage as numeric factors and inlet air as a categorical factor) were investigated by the use of central composition design (CCD), a subclass in RSM, in Design-Expert software. The experiments included eight factorial, eight axial, and six center points. Details of parameters and experimental runs are represented in Tables 1 and 2, respectively. The pH (Factor *A*) range was selected from 7.00 to 10.00, while the range for photocatalyst dosage (Factor *B*) was between 0.2 to 0.4 g. The air flow rate (Factor *C*) entering the photoreactor was set in two minimum and maximum levels.

Finally, a quadratic model [Eq. (3)] has been applied, and the analysis of variance (ANOVA) table (Table 3) was analyzed to fully evaluate the influence of factor interactions and individual parameters. The ANOVA table could be applied to estimate the parameter's significance and goodness of fitting for the predicted model. The optimal amount of each variable was selected due to the desirability function of the suggested model which should be between 0.0 to 1.0 from low to high desirability [52].

$$R = a_0 + \sum a_i X_i + \sum a_{ii} X_i^2 + \sum a_{ij} X_i X_j + \varepsilon \quad (3)$$

where R: predicted result; a_0: intercept coefficient; a_i: linear effect of X_i (=*A*, *B*, and *C*); a_{ii}: quadratic effect of X_i; a_{ij}: linear interaction effect between X_i and X_j (=*A*, *B*, and *C*); ε: residual term.

3. Results and discussion

3.1. Structural characterization

3.1.1. X-ray diffraction analysis

Generally, the Scherrer equation is only suitable when the crystal grain sizes are less than 100 nm. Besides, when the mechanical force is used for the preparation of a composite, the applied force creates some strain on the crystal which causes the change in d-spacing. Based on the Braggs' law ($n\lambda = 2d\sin\theta$), this d fluctuation results in the change in θ. In such a case, the Williamson–Hall (W-H) equation is a better method to investigate the grain size. To study the effects of size and strain broadening on the crystallite size, simultaneously, the W-H equation was used as shown by Eq. (4) [53].

$$\beta_{hkl}\cos\theta = \left(\frac{k\lambda}{d}\right) + 4\varepsilon\sin\theta \quad (4)$$

where the first term in the right hand confirms the Scherrer equation while the second term shows the effect of internal strain (or Stokes and Wilson expression). Commonly, the β-value can be affected by various factors such as the crystallite size, strain, instrumental parameters, and crystal defects. When broadening is independent of 1/*d*, an increase in 1/*d* value increases the effect of the strain broadening. Also, when the strain factor ε is about zero, the net Scherrer equation can be derived from the W-H equation [53].

Williamson–Hall (W-H) equation is a method to investigate the grain size of crystals. When the strain factor in the W-H equation becomes zero Deby–Scherrer equation could be obtained [53]. Despite other reports considering the

Table 1
Levels of factors in central composition design (10 ppm methylene blue concentration)

	Parameter	–1 level	+1 level	–α	+α
A	pH	7	10	6.38	10.62
B	Photocatalyst (g)	0.2	0.4	0.16	0.44
C	Inlet air	Minimum	Maximum	–	–

Table 2
Central composition design matrix and responses

Run number	*A*: pH	*B*: Photocatalyst dosage	*C*: Inlet air	Response[a]
1	8.50	0.30	Max.	0.58
2	8.50	0.30	Min.	2.06
3	8.50	0.16	Max.	2.37
4	10.62	0.30	Max.	2.91
5	8.50	0.44	Min.	1.29
6	10.62	0.30	Min.	13.08
7	10.00	0.20	Min.	13.98
8	8.50	0.30	Min.	1.86
9	10.00	0.20	Max.	6.58
10	8.50	0.16	Min.	7.31
11	8.50	0.44	Max.	1.19
12	7.00	0.40	Min.	2.30
13	7.00	0.20	Min.	2.18
14	7.00	0.20	Max.	1.57
15	10.00	0.40	Min.	3.44
16	8.50	0.30	Max.	0.96
17	10.00	0.40	Max.	0.83
18	7.00	0.40	Max.	0.65
19	6.38	0.30	Max.	0.13
20	6.38	0.30	Min.	0.15
21	8.50	0.30	Min.	2.17
22	8.50	0.30	Max.	0.91

[a]Response is calculated from degradation percentage according to Eq. (2).

Table 3
ANOVA analysis

Source	Sum of squares	DF	Mean square	*F*-value	*P*-value	
Model	307.00	17	18.06	536.39	<0.0001	Significant
A-pH	61.70	1	61.70	1,832.70	<0.0001	
B-Photocatalyst	12.96	1	12.96	384.95	<0.0001	
C-Inlet air	2.21	1	2.21	65.59	0.0013	
AB	29.99	1	29.99	890.87	<0.0001	
AC	25.76	1	25.76	765.02	<0.0001	
BC	5.86	1	5.86	173.95	0.0002	
A^2	16.78	1	16.78	498.41	<0.0001	
B^2	6.27	1	6.27	186.32	0.0002	
ABC	4.25	1	4.25	126.20	0.0004	
A^2B	2.98	1	2.98	88.58	0.0007	
A^2C	9.04	1	9.04	268.53	<0.0001	
AB^2	1.04	1	1.04	31.01	0.0051	
B^2C	1.02	1	1.02	30.43	0.0053	
A^2B^2	0.6006	1	0.6006	17.84	0.0134	
A^2BC	0.5986	1	0.5986	17.78	0.0135	
AB^2C	2.73	1	2.73	80.97	0.0008	
A^2B^2C	0.5476	1	0.5476	16.27	0.0157	
Pure error	0.1347	4	0.0337			
Cor. total	307.13	21				
		Sum of squares is Type III – partial				
Std. Dev.	0.1835		R^2	0.9996		
Mean	3.11		Adjusted R^2	0.9977		
C.V. %	5.89		Adeq. precision	83.4497		

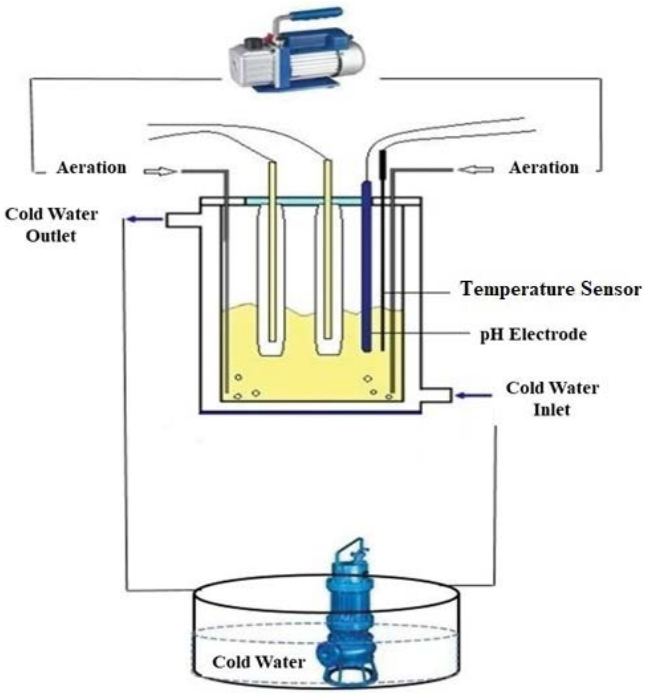

Fig. 2. Photoreactor schematic.

Deby–Scherrer equation for particle size calculations, the equation could not be suitably applied to ZIF-11. This is due to the Deby–Scherrer validity for particles smaller than 1 μ [54], which cannot be reasonable to perform for this photocatalyst due to particle size observations in the FESEM result.

Experimental data from XRD pattern shown in Fig. 3, is in excellent accordance with the ones reported in the literature. The pattern peaks at 2θ° of 4.31°, 6.03°, and 7.52°. The characteristic peaks match well with the reported XRD patterns by Boroglu and Ahenk [39] and Hu et al. [37]. This indicates ideal internal structure in the sample which has been successfully synthesized. High crystallinity and rhombic dodecahedron (RHO) type morphology can be best observed according to the ZIF-11 XRD pattern.

3.1.2. FESEM analysis

Fig. 4 represents the FESEM analysis results of ZIF-11 crystals. The figure exhibits great RHO topology, and the particle size was almost about 0.5 to 6 μm which is in good match with the reported data [41]. The average size is estimated to be approximately 2.5 μm.

3.1.3. Energy-dispersive X-ray analysis

EDX analysis confirms the purity of the ZIF-11 crystal phase. Four different molecules were identified in the ZIF-11

structure due to the EDX analysis taken. All four observed molecules were expected to occur in the EDX test in accordance with the initial raw material applied in the synthesis procedure (Fig. 5). The highest weight percentage, which was 59.35% belonged to carbon. Nitrogen, oxygen, and zinc compositions were reported to be 27.10%, 1.51%, and 12.60%, respectively. There was no sign of impurity due to the absence of any other molecules in this test.

3.1.4. Brunauer–Emmett–Teller analysis

The nano-structural phase was proven from the BET average pore diameter, which is 1.98 nm (Fig. 6). Nitrogen adsorption–desorption isotherms in 77 k indicate the ZIF-11 isotherm is categorized as type I. This is a sign of a microporous structure. The hysteresis loop occurring in the isotherm curves was H4 type in IUPAC classifications. This shows meso-structure crystals restricting by dominantly microstructural ones in ZIF-11 nature. The interaction between pore walls and adsorbate is an obvious reaction in the adsorption process. The very low partial pressures (0.3 bar) provide better adsorption reactions. BET surface area and total pore volume are reported to be 378 m^2/g and 185 mm^3/g, respectively.

3.1.5. Fourier-transform infrared spectroscopy

Fig. 7 exhibits the molecular bands between components consisting of ZIF-11, and Fig. 8 shows the peaks that occurred in FTIR analysis of ZIF-11. Peaks at 3,029.96; 3,062.75 and

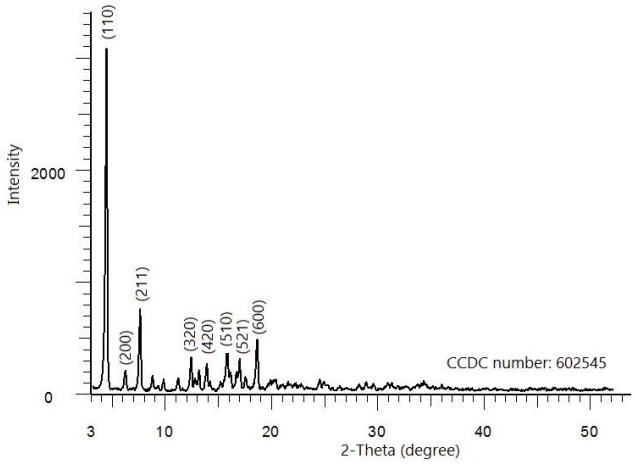

Fig. 3. X-ray diffraction pattern of ZIF-11 crystals.

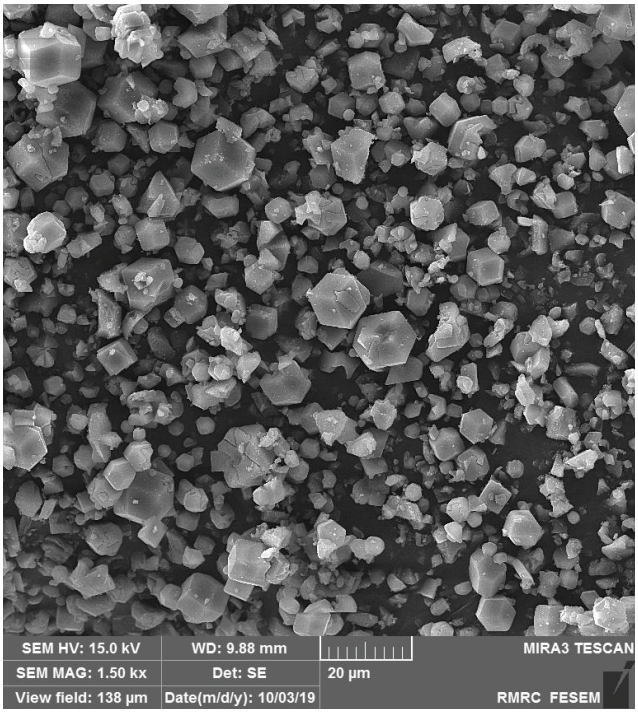

Fig. 4. Field emission scanning electron microscopy image of ZIF-11 crystals representing; the distribution of crystals.

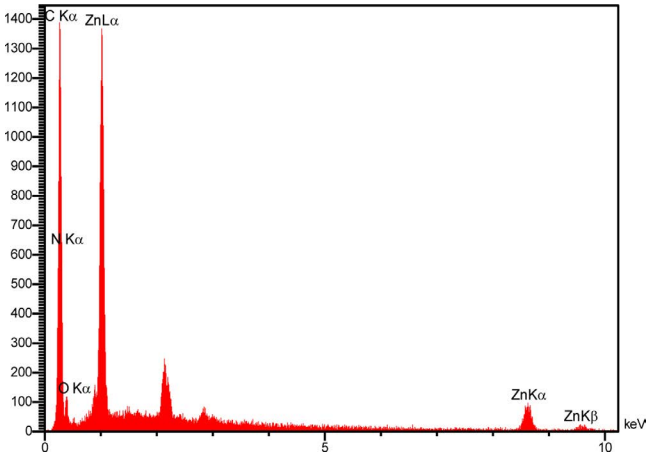

Fig. 5. Energy-dispersive X-ray spectroscopy analysis of ZIF-11.

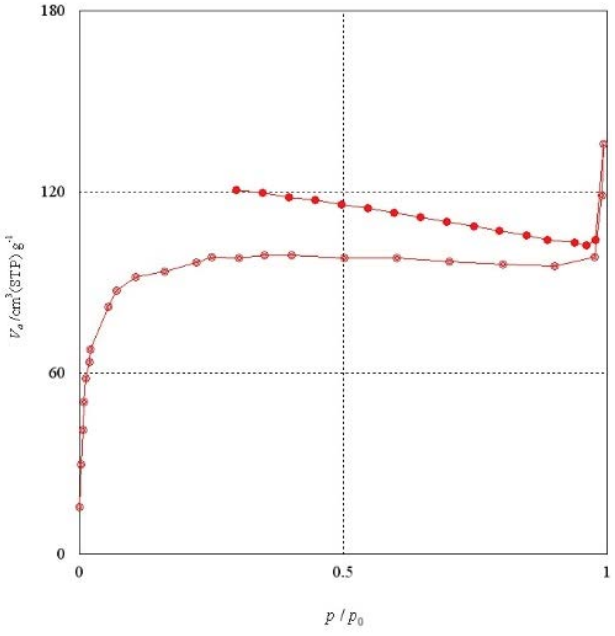

Fig. 6. Brunauer–Emmett–Teller analysis of ZIF-11.

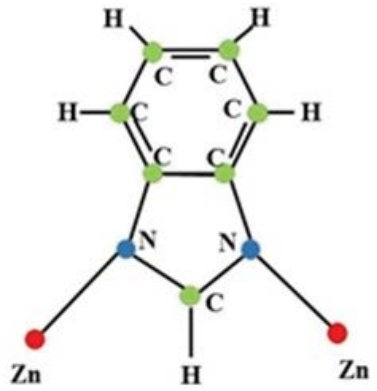

Fig. 7. Molecular bonding in ZIF-11.

3,082.04 cm^{-1} indicated the bonding between C–H. The peaks at a wavenumber of 1,467 and 1,610 cm^{-1} are attributed to the stretching of C–C in the benzimidazole aromatic ring [55]. The bonding between C–N and Zn–N is observed at 1,280.65 and 424.31 cm^{-1}, respectively [55]. The only unexpected sign of bonding is estimated to be for C–O in 1,244 cm^{-1}, which could be because of the bond between carbon in benzimidazole and oxygen in methanol.

3.1.6. Differential reflectance spectroscopy

Approximate photocatalytic activity was observed to be in 250 to 300 nm, which is in the UV-C region from the DRS analysis (Fig. 9). The other fact calculated from the data reported in this test is the band gap of ZIF-11.

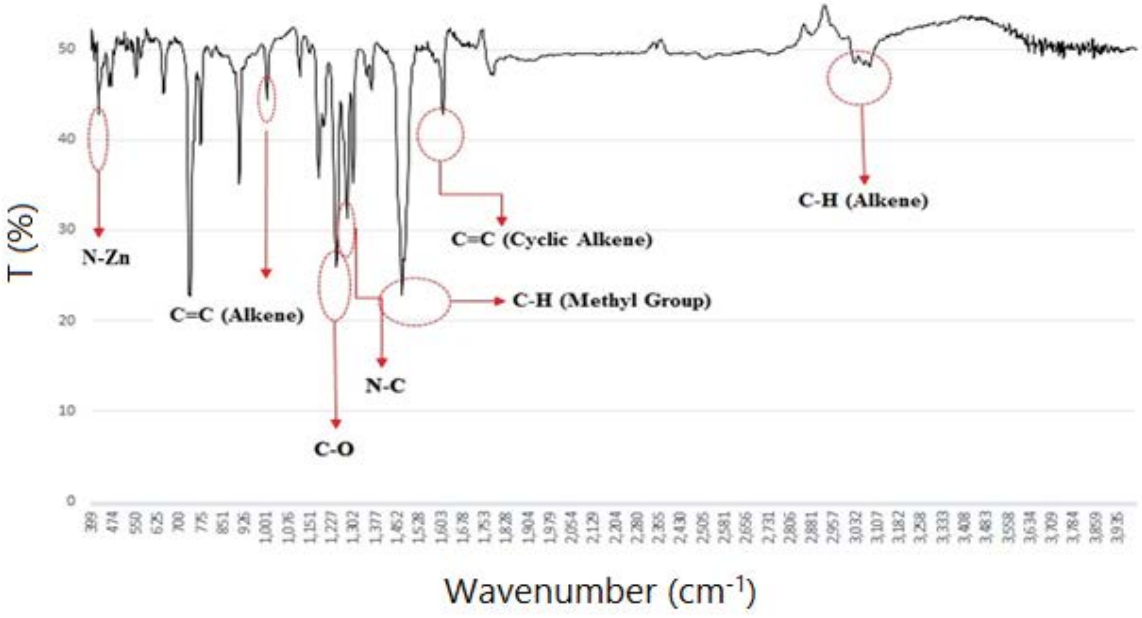

Fig. 8. Fourier-transform infrared spectra of ZIF-11.

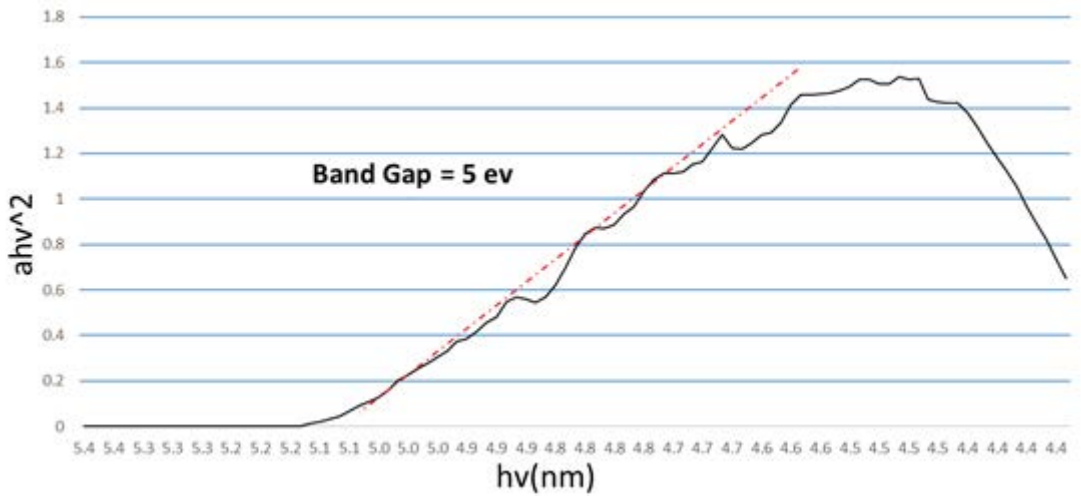

Fig. 9. ZIF-11 Tauc plot.

Kubelka–Munk equation provides the conversion of reflectance data into a parameter named *K*, which is proportional to the rate between absorption and scattering coefficient *K* [Eq. (5)] is considered as reflectance transformed according to Kubelka–Munk equation where *R* is the reflectance obtained using UV-Vis spectra [56]. The band gap in this study has been calculated using the Tauc plot. The mentioned plot was provided by plotting the amounts of $(\alpha h\upsilon)^{1/2}$ vs. $h\upsilon$. The band gap of 5.0 eV is in good match with the band gap reported for ZIF-8 [43].

$$K = \frac{\left(1-R\right)^2}{2R} \tag{5}$$

3.1.7. Hydrophobicity nature of ZIF-11

The hydrophobic behavior of ZIF-11 was considered through a test measuring the contact angle between compact powder and water. The average contact angle observed was about 166°, which is a sign of extreme hydrophobicity. Although being hydrophobic for a photocatalyst performing in water seems to be a drawback, this characteristic would be an advantage in the separation process after the reaction is completed.

3.2. Photocatalytic performance

The photoactivity of as-synthesized ZIF-11 was evaluated through a dye degradation process. To ensure the reaction was neither catalytic nor photolysis, it was done once in the mere presence of ZIF-11 in darkness and another time by applying UV lights without using the photocatalyst. The result expressed no significant degradation by applying both methods. Therefore, the reaction turned out to be photocatalytic, and consequently, the applicability of ZIF-11 as a photocatalyst was proved. In addition, functional groups and unsaturated metal atoms on organic ligands can be used as catalytic activity centers [57].

3.2.1. Analysis of variance

The design of experiments led to 22 photocatalytic runs for further investigation of operational parameters and their effect on the degradation process. Factors with larger *F*-values and *P*-values less than 0.05 are recognized as the most significant ones [58,59]. Dividing the model mean square by the residual mean square results in the calculated model *F*-value. Table 3 is the ANOVA analysis, which exhibits an insignificant lack-of-fit, which is a sign of an adequate model [52]. The quadratic equation obtained according to ANOVA analysis:

$$\begin{aligned} R = {} & 1.42 + 2.78A - 1.27B - 0.61C - 1.94AB - 1.79AC \\ & + 0.86BC + 1.32A^2 + 0.81B^2 + 0.73ABC - 0.86A^2B \\ & - 0.97A^2C - 0.51AB^2 - 0.33B^2C + 0.39A^2B^2 \\ & - 0.39A^2BC + 0.82AB^2C + 0.37A^2B^2C \end{aligned} \tag{6}$$

The *R*-squared and adjusted *R*-squared of the model were reported to be 0.9996 and 0.9977, respectively which can ensure the model's validity. The validity of the model could also be indicated by the amount of *F*-value which is significant enough [56]. The *P*-value of the model is less than 0.0001 which is a sign of a good model. The number calculated for adequate precision by the model is 83.4497. Adequate precision of more than 4 represents the sufficiency and adequacy of the model.

3.2.2. Residual plots

Fig. 10 illustrates the perfect match between the calculated or predicted result and the actual result. It is indicated that the mentioned results are located around the bisector line which is a sign of an adequate and precise model. The other significant plot is the residual plot which is shown in Fig. 11. In this figure, the independence of the obtained results and reaction run number is observed. Thus, it can be gained from the figure that the residual amount is properly distributed.

3.3. Operational parameters

Numerical factors investigated in this research study include pH and photocatalyst dosage. The range of these two parameters has been chosen by previous experiments. The pH range was selected to be from 7.00 to 10.00, while the range for dosage was between 0.2 to 0.4 g. It is noteworthy to mention that some experiments were done out of this range as the Design-Expert software suggestion. This step was necessary for modeling and further optimization. The other investigated parameter was the air flow rate entering the photoreactor, which was considered to be a categorical factor and set in two different levels (minimum and maximum).

3.3.1. Effect of initial pH on MB degradation

The calculated *R* showed a significant increase with the increase in pH amount (Fig. 12). This is in direct relation

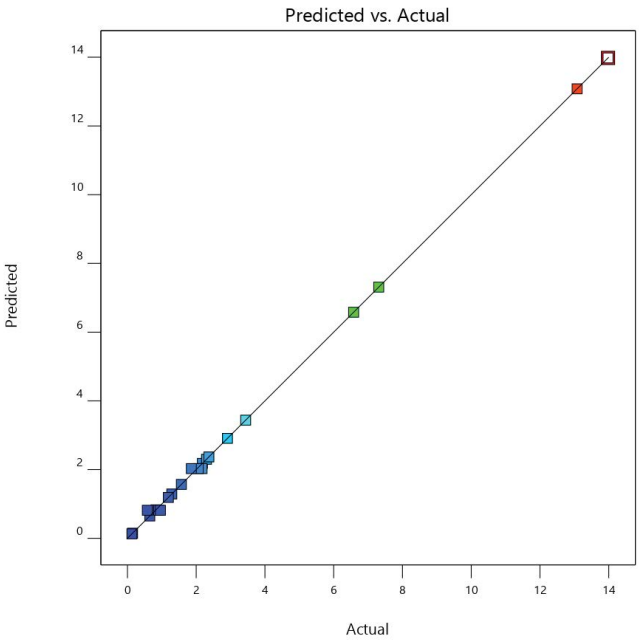

Fig. 10. Predicted vs. actual data.

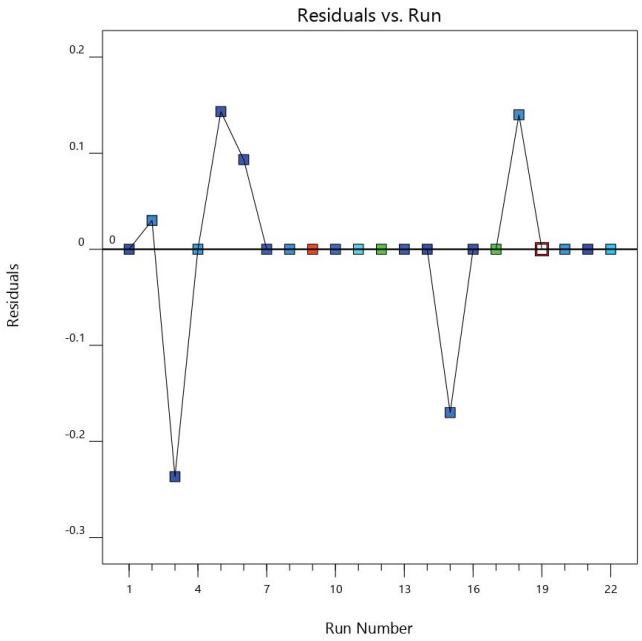

Fig. 11. Residual plot vs. run number.

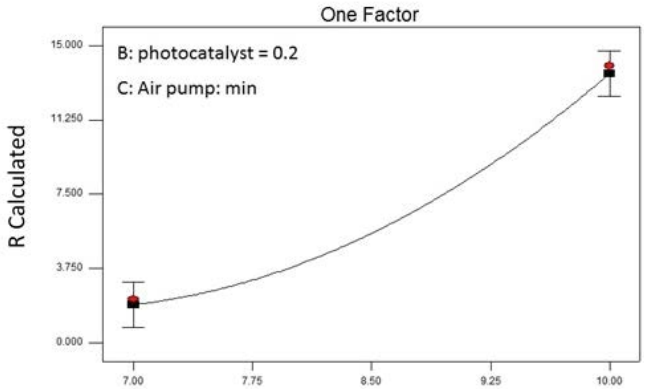

Fig. 12. Effect of pH on response (air pump: min and photocatalyst dosage: 0.2).

with the pH_{pzc} of ZIF-11. As ZIF-11 pH_{pzc} was 6.4, the behavior of its surface is estimated to be eager to adsorb particles with positive charges at basic conditions (greater than 6.4). Considering the effect of pH on the surface charge characteristics, on one hand, and very low pKa (less than 1) of MB as a cationic dye, on the other hand, better degradation performance in basic conditions is achieved. This issue is because of better absorbance of effluent and a more effective degradation process in the cationic medium [43,60]. The same results were obtained by applying ZIF-8 as a photocatalyst to degrade MB under UV radiation. The degradation process showed better performance in alkaline media with pH amounts of 12 [43]. The other reason for greater degradation in basic mediums could be attributed to the further suspension of ZIF-11 in the MB solution. Previous reports indicated the influence of pH on nanomaterial suspension in aqueous media [61,62]. This was observed in the experiments done in this study by having

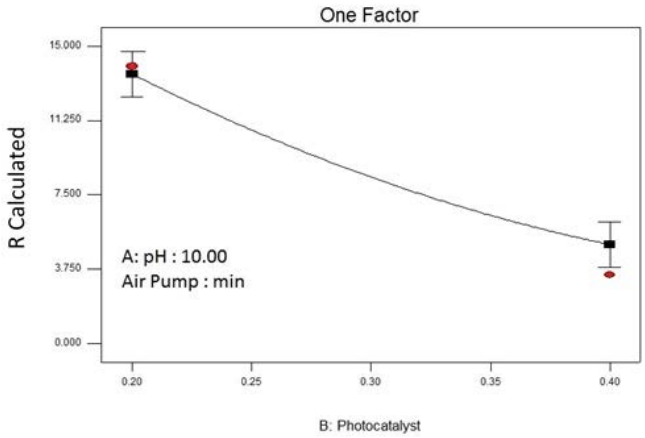

Fig. 13. Effect of photocatalyst on response (air pump: min and pH value: 10).

more powder attached to walls and on the top of the reactor while working at a lower pH. Moreover, the photoactivity of a catalyst in alkaline mediums is known to be an advantage because of the basic nature of most hazardous organic wastes, including dyes and caustics [63].

3.3.2. Effect of photocatalyst dosage on degradation process

Several experiments were done with different photocatalyst dosages suggested by Design-Expert in the range of 0.16–0.44 g (Fig. 13). The results exhibited the optimum amount of ZIF-11 for this degradation to be 0.2 g in a 300 mL MB solution. The amounts below 0.2 g are too low to be capable of decomposing dangerous components consisting of waste sewage. This was predicted because of having insufficient active sites on the photocatalyst surface available to participate in the reaction [64]. It was also found from the experimental results that photocatalyst usages above 0.2 g were not improving the reaction process. The reason is the sedimentation and agglomeration occurring in the photoreactor. Besides, having higher amounts of ZIF-11 in the reactor will cause turbidity, therefore the light access to MB species is limited to make them thoroughly decomposed [65–67].

3.3.3. Effect of inlet air flow rate

The inlet air was set on the actual degrees of minimum and maximum (Fig. 14). All the experiments done at minimum air flow rate showed better degradation results than the ones carried out at maximum flow. One of the reasons leading to this observation would be the larger air bubble sizes entering the reaction zone, which consequently reduces the required surface area for performing the photodegradation process. The larger bubbles produced, have less remaining time in the photoreactor, which minimizes the chance of oxidation–reduction reactions [67,68]. It is worth to mentioning that when applying hydrophobic photocatalysts, the entrance of higher airflow to the reactor increases ZIF-11 particle's tendency to stay on the surface of the reactor rather than the middle of the solution. For this reason, there would not be enough photocatalysts to perform the degradation and decomposition reaction [61,69].

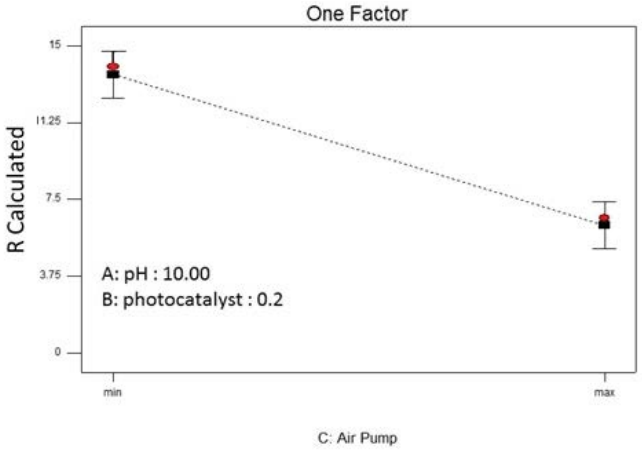

Fig. 14. Effect of air flow rate on response (pH value: 10 and photocatalyst dosage: 0.2).

3.3.4. Optimum amounts of operational parameters

The optimal result was achieved when the maximum *R* and minimum amount of photocatalyst dosage were set in the optimization section of Design-Expert software. The best result was for the experiment in which the pH and photocatalyst dosage were respectively 10.0 and 0.2 g, and the airflow rate was set at the minimum amount. Specified operational parameters resulted in a degradation percentage of 82.88% in 30 min of UV light irradiation. Fig. 15 exhibits the mentioned result. The obtained degradation percentage (82.88%) was approximately close to the amount achieved by Jing et al. [43] (82.3%) who applied ZIF-8 to photodegrade MB under UV light. The significant difference between the present work and the reported one is light source power (500 W for ZIF-8 and 24 W for ZIF-11). Applying low-power lamps would be economically and environmentally beneficial. Furthermore, the reaction time in the previous study under UV light irradiation was longer (120 min) than the present work which was 30 min. The above-mentioned facts which were related to time and energy-saving aspects, indicate more impressive results in this study. Also, the perturbation plots of parameters are given in Figs. 16 and 17.

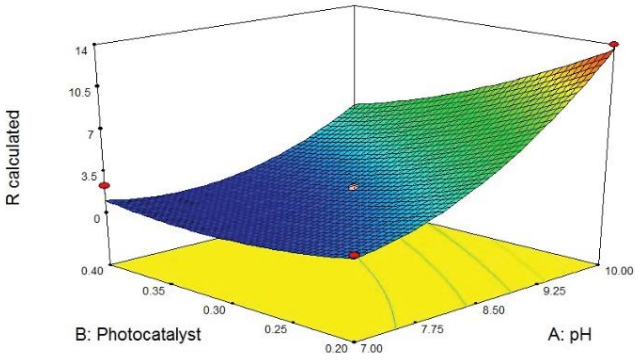

Fig. 15. Optimum amounts of pH-photocatalyst dosage in minimum air flow rate.

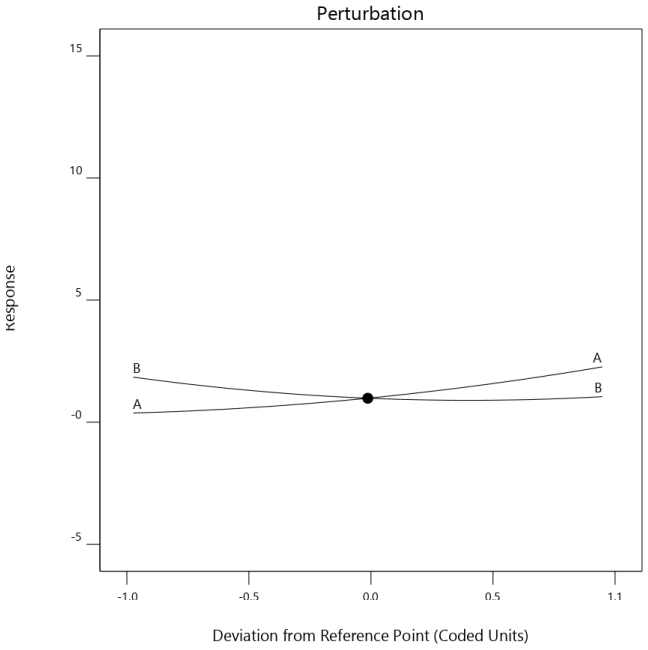

Fig. 16. Perturbation plot at *A*: pH = 8.5, *B*: photocatalyst = 0.3, *C* = inlet air = max.

3.4. Kinetic study of the reaction

The prepared photocatalyst in this study followed the Langmuir–Hinshelwood (L-H) model, which is an accepted model for the kinetic study of degradation processes in metal–organic frameworks [70,71]. Therefore, the kinetics of ZIF-11 degradation of MB:

$$y = -\frac{dC}{dt} = kC \tag{7}$$

$$\ln\frac{C_0}{C} = kt \tag{8}$$

where *y*, *C*, and *k* represent the kinetic rate, MB concentration, and the apparent rate constant, respectively. Fitting the $\ln(C/C_0)$ vs. the time plot expressed that the MB degradation mechanism using ZIF-11 was perfectly following the Langmuir–Hinshelwood kinetic model. Fig. 18 represents $\ln(C/C_0)$ vs. time plot with R^2 of 0.9382 which indicates the pseudo-first-order kinetic model. The slope of this plot which is 0.0309 min^{-1} is the apparent rate constant.

As stated in most literature, holes generated in ZIF-11 photocatalyst in the presence of UV light irradiation would react with the MB solution to form hydroxyl and superoxide radicals. The photogenerated radicals might then decompose dye molecules to form intermediate products known as organic acids. Since organic dye and ZIF-11 had primarily been mixed in the dark for 30 min to activate photocatalyst particles, the first step in the photodegradation mechanism would be the adsorption process [20,72]. The other photocatalytic reaction decomposition is listed in relative references [3,73]. Some intermediate products may also occur which have been investigated in literature by GC-MS and ion chromatography results in the photodegradation of MB [74].

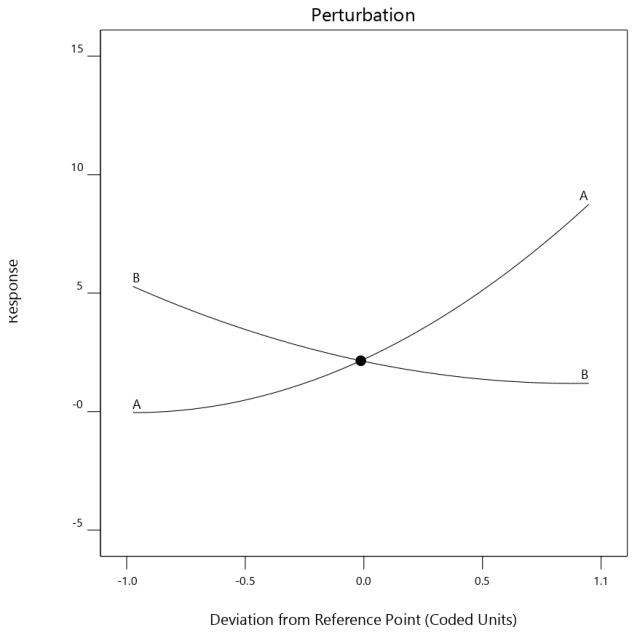

Fig. 17. Perturbation plot at *A*: pH = 8.5, *B*: photocatalyst = 0.3, *C* = inlet air = min.

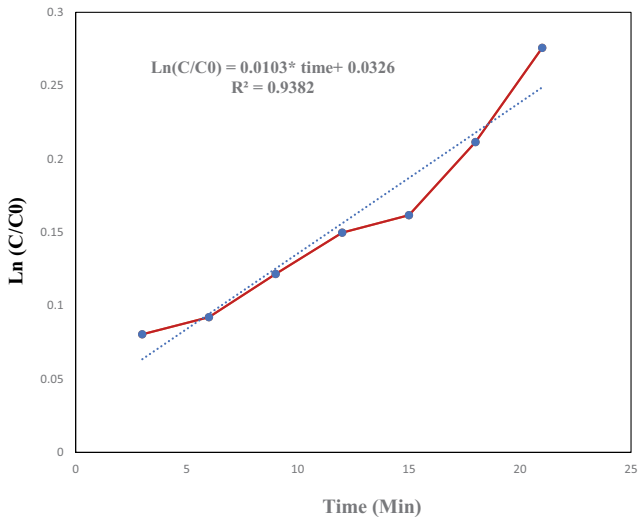

Fig. 18. Apparent rate constant calculation.

4. Conclusion

The novel photocatalytic application of ZIF-11 crystals under UV irradiation was successfully performed and resulted in excellent dye degradation. The photocatalyst synthesis was pursued via a facile Solvothermal method. The photocatalytic reaction was performed in a photoreactor in which methylene blue was used as an organic effluent. Different operational parameters including pH, photocatalyst dosage, and airflow rate entering the reactor were investigated through a CCD method in Design-Expert software. Subsequently, pH was recognized as the most effective factor, furthermore, improvements in the degradation process occurred while working in more basic conditions. Ultimately, a theoretical quadratic model was suggested from the software which makes it possible to investigate the optimization of the discussed process, deeply. Therefore, taking advantage of a metal–organic framework in the photodegradation process of organic waste was carried out and it is anticipated to be expanded in more empirical executions.

References

[1] Y. Pi, L. Xiyi, X. Qibin, W. Junliang, L. Yingwei, X. Jing, L. Zhong, Adsorptive and photocatalytic removal of persistent organic pollutants (POPs) in water by metal–organic frameworks (MOFs), Chem. Eng. J., 337 (2018) 351–371.
[2] P. Kumar, B. Vasudha, K. Ki-Hyun, E.K. Eilhann, Metal–organic frameworks (MOFs) as futuristic options for wastewater treatment, J. Ind. Eng. Chem., 62 (2018) 130–145.
[3] V. Sharma, K. Virender, F. Mingbao, Water depollution using metal–organic frameworks-catalyzed advanced oxidation processes: a review, J. Hazard. Mater., 372 (2019) 3–16.
[4] S. Hashemi, A. Nezamzadeh-Ejhieh, A novel chromium selective electrode based on surfactant-modified Iranian clinoptilolite nanoparticles, Desal. Water Treat., 57 (2016) 3304–3314.
[5] Z. Abbasi, C. Levente, Z. Xiwang, P.L. Bradley, W. Huanting, Metal–Organic Frameworks (MOFs) and MOF-Derived Porous Carbon Materials for Sustainable Adsorptive Wastewater Treatment, G. Szekely, A. Livingston, Eds., Sustainable Nanoscale Engineering: From Materials Design to Chemical Processing, Elsevier, Amsterdam, The Netherlands, 2020, pp.163–194.
[6] K. Paździor, L. Bilińska, S. Ledakowicz, A review of the existing and emerging technologies in the combination of AOPs and biological processes in industrial textile wastewater treatment, Chem. Eng. J., 376 (2019) 120597, doi: 10.1016/j.cej.2018.12.057.
[7] S. Mousavi-Mortazavi, A. Nezamzadeh-Ejhieh, Supported iron oxide onto an Iranian clinoptilolite as a heterogeneous catalyst for photodegradation of furfural in a wastewater sample, Desal. Water Treat., 57 (2016) 10802–10814.
[8] Z.A. Mirian, A. Nezamzadeh-Ejhieh, Removal of phenol content of an industrial wastewater via a heterogeneous photodegradation process using supported FeO onto nanoparticles of Iranian clinoptilolite, Desal. Water Treat., 57 (2016) 16483–16494.
[9] A. Lajevardi, M.T. Yaraki, A. Masjedi, A. Nouri, M.H. Sadr, Green synthesis of MOF@Ag nanocomposites for catalytic reduction of methylene blue, J. Mol. Liq., 276 (2019) 371–378.
[10] N.T. Tran, K. Daekeun, S.Y. Kye, K. Jinsoo, Synthesis of Cu-doped MOF-235 for the degradation of methylene blue under visible light irradiation, Bull. Korean Chem. Soc., 40 (2019) 112–117.
[11] Y. Ren, L. Ting, Z. Weiming, W. Shu, S. Mengqi, S. Chao, Z. Wenbin, MIL-PVDF blend ultrafiltration membranes with ultrahigh MOF loading for simultaneous adsorption and catalytic oxidation of methylene blue, J. Hazard. Mater., 365 (2019) 312–321.
[12] Y. Tan, S. Zhongqiao, M. Hao, H. Yide, W. Junbiao, X. Junli, X. Yan, Z. Xia, A new MOFs/polymer hybrid membrane: MIL-68 (Al)/PVDF, fabrication and application in high-efficient removal of p-nitrophenol and methylene blue, Sep. Purif. Technol., 215 (2019) 217–226.
[13] J. Panda, K.S. Jitendra, K.P. Prasanna, N.S. Satya, S. Mahalaxmi, K.P. Subrat, S. Rojalin, Adsorptive behavior of zeolitic imidazolate framework-8 towards anionic dye in aqueous media: combined experimental and molecular docking study, J. Mol. Liq., 278 (2019) 536–545.
[14] N. Tu, T. Thi, V.T. Tran, D.D. Pham, T.T.C Vo, X. M Tran, Q.K. Dinh, Adsorptive removal of Congo red from aqueous solution using zeolitic imidazolate framework–67, J. Environ. Chem. Eng., 6 (2018) 2269–2280.
[15] W.L. Wang, C. Yi-Zhong, H. Hong-Ying, C. Jian, W. Jing, X. Gang, W. Qian-Yuan, Advanced treatment of bio-treated dyeing and finishing wastewater using ozone-biological activated carbon: a study on the synergistic effects, Chem. Eng. J., 359 (2019) 168–175.

[16] Z. Kiayi, T. Bagherilotfabad, A. Heidarinasab, F. Shahcheraghi, Microbial degradation of azo dye carmoisine in aqueous medium using *Saccharomyces cerevisiae* ATCC 9763, J. Hazard. Mater., 373 (2019) 608–619.
[17] R. Pešoutová, P. Hlavínek, J. Matysíková, Use of advanced oxidation processes for textile wastewater treatment–a review, Food Environ. Saf. J., 10 (2017) 59–65.
[18] M. Gągol, P. Andrzej, B. Grzegorz, Wastewater treatment by means of advanced oxidation processes based on cavitation–a review, Chem. Eng. J., 338 (2018) 599–627.
[19] M. Asgharian, M. Mehdipourghazi, B. Khoshandam, N. Keramati, Photocatalytic degradation of methylene blue with synthesized rGO/ZnO/Cu, Chem. Phys. Lett., 719 (2019) 1–7.
[20] A.G. Akerdi, S. Hajir Bahrami, Application of heterogeneous nano-semiconductors for photocatalytic advanced oxidation of organic compounds: a review, J. Environ. Chem. Eng., 7 (2019) 103283, doi: 10.1016/j.jece.2019.103283.
[21] D.V. Miklos, R. Christian, J. Martin, G.L. Karl, E.D. Jörg, H. Uwe, Evaluation of advanced oxidation processes for water and wastewater treatment–a critical review, Water Res., 139 (2018) 118–131.
[22] D. Jiang, X. Piao, W. Han, Z. Guangming, H. Danlian, C. Ming, L. Cui, Z. Chen, J. Wan, X. Wenjing, Strategies to improve metal organic frameworks photocatalyst's performance for degradation of organic pollutants, Coord. Chem. Rev., 376 (2018) 449–466.
[23] J. Qiu, Z. Xingguang, F. Yi, Z. Xiongfei, W. Huanting, Y. Jianfeng, Modified metal-organic frameworks as photocatalysts, Appl. Catal., B, 231 (2018) 317–342.
[24] M. Hossein Zadeh, N. Keramati, M. Mehdipour Ghazi, Ultrasonic-assisted synthesis of new photocatalyst based on Fe–benzenetricarboxylic (Fe–BTC) metal organic framework: characterization and photocatalytic properties, J. Iran. Chem. Soc., 16 (2019) 401–409.
[25] X. Deng, H. Mingming, L. Zhaohui, Engineering metal–organic frameworks (MOFs) for efficient photocatalysis, Curr. Org. Chem., 22 (2018) 1825–1835.
[26] A. Kirchon, F. Liang, F.D. Hannah, A.J. Elizabeth, H.-C. Zhou, From fundamentals to applications: a toolbox for robust and multifunctional MOF materials, Chem. Soc. Rev., 47 (2018) 8611–8638.
[27] H. Derikvandi, A. Nezamzadeh-Ejhieh, Increased photocatalytic activity of NiO and ZnO in photodegradation of a model drug aqueous solution: effect of coupling, supporting, particles size and calcination temperature, J. Hazard. Mater., 321 (2017) 629–638.
[28] J. Esmaili-Hafshejani, A. Nezamzadeh-Ejhieh, Increased photocatalytic activity of Zn(II)/Cu(II) oxides and sulfides by coupling and supporting them onto clinoptilolite nanoparticles in the degradation of benzophenone aqueous solution, J. Hazard. Mater., 316 (2016) 194–203.
[29] B. Seoane, M.Z. Juan, T. Carlos, C. Joaquin, Sonocrystallization of zeolitic imidazolate frameworks (ZIF-7, ZIF-8, ZIF-11 and ZIF-20), Cryst. Eng. Commun., 14 (2012) 3103–3107.
[30] K.S. Park, N. Zheng, P.C. Adrien, Y.C. Jae, H. Rudan, J.U-R. Fernando, K.C. Hee, O. Michael, M.Y. Omar, Exceptional chemical and thermal stability of zeolitic imidazolate frameworks, Proc. Natl. Acad. Sci. U.S.A., 103 (2006) 10186–10191.
[31] B. Reif, F. Florian, H. Maximilian, H. Martin, S. Wilhelm, Synthesis of ZIF-11 – effect of water residues in the solvent onto the phase transition from ZIF-11 to ZIF-7-III, Microporous Mesoporous Mater., 243 (2017) 65–68.
[32] B. Reif, P. Carolin, F. Florian, H. Martin, K. Malte, S. Wilhelm, Synthesis of ZIF-11 – influence of the synthesis parameters on the phase purity, Microporous Mesoporous Mater., 275 (2019) 102–110.
[33] S.S. Han, C. Seung-Hoon, A.G. William, Zeolitic imidazolate frameworks as H_2 adsorbents: *Ab initio* based grand canonical monte carlo simulation, J. Phys. Chem. C, 114 (2010) 12039–12047.
[34] W. Wongsinlatam, T. Remsungnen, Molecular dynamics simulations of CO_2 molecules in ZIF-11 using refined AMBER force field, J. Chem., 2013 (2013) 415027, doi: 10.1155/2013/415027.
[35] R. Chen, Y. Jianfeng, G. Qinfen, S. Stef, B. Christian, G. Haoxue, Z. Dunru, M. William, O.M. Yaghi, W. Huanting, A two-dimensional zeolitic imidazolate framework with a cushion-shaped cavity for CO_2 adsorption, Chem. Commun., 49 (2013) 9500–9502.
[36] A. Phan, J.D. Christian, J.U.R. Fernando, B.K. Carolyn, O. Michael, M.O. Yaghi, Synthesis, structure, and carbon dioxide capture properties of zeolitic imidazolate frameworks, Acc. Chem. Res., 43 (2010) 58–67.
[37] H. Hu, L. Shengquan, C. Chunyan, W. Jianping, Z. Ying, L. Lihua, Y. Shouzhuo, Two novel zeolitic imidazolate frameworks (ZIFs) as sorbents for solid-phase extraction (SPE) of polycyclic aromatic hydrocarbons (PAHs) in environmental water samples, Analyst, 139 (2014) 5818–5826.
[38] A.W. Thornton, D. David, S.L. Ming, P.L. Bradley, J.H. Anita, R.H. Matthew, Feasibility of zeolitic imidazolate framework membranes for clean energy applications, Energy Environ. Sci., 5 (2012) 7637–7646.
[39] M.S. Boroglu, B.Y. Ahenk, Gas separation performance of 6FDA-DAM-ZIF-11 mixed-matrix membranes for H_2/CH_4 and CO_2/CH_4 separation, Sep. Purif. Technol., 173 (2017) 269–279.
[40] A. Ehsani, M. Pakizeh, Synthesis, characterization and gas permeation study of ZIF-11/Pebax® 2533 mixed matrix membranes, J. Taiwan Inst. Chem. Eng., 66 (2016) 414–423.
[41] L. Li, Y. Jianfeng, W. Xiaojing, C. Yi-Bing, W. Huanting, ZIF-11/polybenzimidazole composite membrane with improved hydrogen separation performance, J. Appl. Polym. Sci., 131 (2014), doi: 10.1002/app.41056.
[42] E.M. Forman, B. Amineh, F. Lei, J.Z. Kirk, Z. Erkang, Z. Fengyi, P.L. Ryan, V. Sergey, Ethylene diffusion in crystals of zeolitic imidazole framework-11 embedded in polymers to form mixed-matrix membranes, Microporous Mesoporous Mater., 274 (2019) 163–170.
[43] Jing, P. Huan, W. Chong-Chen, Z. Yi-Wen, W. Peng, L. Ran, Photocatalytic degradation of methylene blue in ZIF-8, RSC Adv., 4 (2014) 54454–54462.
[44] K.-Y.A. Lin, C. Hsuan-Ang, Zeolitic imidazole framework-67 (ZIF-67) as a heterogeneous catalyst to activate peroxymonosulfate for degradation of Rhodamine B in water, J. Taiwan Inst. Chem. Eng., 53 (2015) 40–45.
[45] N.M. Mahmoodi, J. Abdi, Nanoporous metal-organic framework (MOF-199): synthesis, characterization and photocatalytic degradation of Basic Blue 41, Microchem. J., 144 (2019) 436–442.
[46] N M. Mahmoodi, J. Abdi, M. Oveisi, M. Alinia Asli, M. Vossoughi, Metal-organic framework (MIL-100 (Fe)): synthesis, detailed photocatalytic dye degradation ability in colored textile wastewater and recycling, Mater. Res. Bull., 100 (2018) 357–366.
[47] R. Liang, J. Fenfen, S. Lijuan, Q. Na, W. Ling, MIL-53 (Fe) as a highly efficient bifunctional photocatalyst for the simultaneous reduction of Cr(VI) and oxidation of dyes, J. Hazard. Mater., 287 (2015) 364–372.
[48] S. Ghattavi, A. Nezamzadeh-Ejhieh, GC-MASS detection of methyl orange degradation intermediates by AgBr/g-C_3N_4: experimental design, bandgap study, and characterization of the catalyst, Int. J. Hydrogen Energy, 45 (2020) 24636–24656.
[49] M. He, Y. Jianfeng, L. Qi, Z. Zhaoxiang, W. Huanting, Toluene-assisted synthesis of RHO-type zeolitic imidazolate frameworks: synthesis and formation mechanism of ZIF-11 and ZIF-12, J. Chem. Soc. Dalton Trans., 42 (2013) 16608–16613.
[50] K.K. Gangu, M. Suresh, S. Babu Mukkamala, S.B. Jonnalagadda, A review on contemporary metal–organic framework materials, Inorg. Chim. Acta, 446 (2016) 61–74.
[51] S. Senobari, A. Nezamzadeh-Ejhieh, A comprehensive study on the photocatalytic activity of coupled copper oxide-cadmium sulfide nanoparticles, Spectrochim. Acta, Part A, 196 (2018) 334–343.
[52] S. Mosleh, M.R. Rahimi, M. Ghaedi, K. Dashtian, Sonophotocatalytic degradation of trypan blue and vesuvine dyes in the presence of blue light active photocatalyst of Ag_3PO_4/Bi_2S_3-HKUST-1-MOF: central composite optimization and synergistic effect study, Ultrason. Sonochem., 32 (2016) 387–397.

[53] A. Noruozi, A. Nezamzadeh-Ejhieh, Preparation, characterization, and investigation of the catalytic property of α-Fe_2O_3-ZnO nanoparticles in the photodegradation and mineralization of methylene blue, Chem. Phys. Lett., 752 (2020) 137587, doi: 10.1016/j.cplett.2020.137587.
[54] R. Sharma, D.P. Bisen, S Usha, B.G. Sharma, X-ray diffraction: a powerful method of characterizing nanomaterials, Recent Res. Sci. Technol., 4 (2012) 77–79.
[55] J. Cheng, M. Dan, L. Shaoxiang, Q. Wenjuan, W. Dong, Preparation of zeolitic imidazolate frameworks and their application as flame retardant and smoke suppression agent for rigid polyurethane foams, Polymers, 12 (2020) 347, doi: 10.3390/polym12020347.
[56] S. Jafari, A. Nezamzadeh-Ejhieh, Supporting of coupled silver halides onto clinoptilolite nanoparticles as simple method for increasing their photocatalytic activity in heterogeneous photodegradation of mixture of 4-methoxy aniline and 4-chloro-3-nitro aniline, J. Colloid Interface Sci., 490 (2017) 478–487.
[57] Y.H. Si, L. Ya-yun, X. Yu, S. Shao-ke, X. Xin-bo, Z. Xie-rong, Z. Ji, Fabrication of novel ZIF-8@$BiVO_4$ composite with enhanced photocatalytic performance, Crystals, 8 (2018) 432, doi: 10.3390/cryst8110432.
[58] D. Hou, G. Ronn, W. Xiaoping, W. Penghua, L. Teik-Thye, Preparation of carbon-sensitized and Fe–Er co-doped TiO_2 with response surface methodology for Bisphenol A photocatalytic degradation under visible-light irradiation, Appl. Catal., B, 126 (2012) 121–133.
[59] T. Olmez-Hanci, I. Arslan-Alaton, B. Gulcan, Multivariate analysis of anionic, cationic and nonionic textile surfactant degradation with the H_2O_2/UV-C process by using the capabilities of response surface methodology, J. Hazard. Mater., 185 (2011) 193–203.
[60] F. Jing, L. Ruowen, X. Jinhua, C. Rui, Z. Shiying, L. Yanhua, W. Ling, MIL-68 (Fe) as an efficient visible-light-driven photocatalyst for the treatment of a simulated wastewater contain Cr(VI) and malachite green, Appl. Catal., B, 206 (2017) 9–15.
[61] A.F. Rawle, Characterization of Nanomaterials, Metrology and Standardization of Nanotechnology: Protocols and Industrial Innovations, Wiley, USA, 2017, pp. 129–150.
[62] K. Min, H.H. Tae, K. Joohoon, J. Jiyoung, J. Cheolsoo, M.H. Soon, M.K. Koo, A facile route to fabricate stable reduced graphene oxide dispersions in various media and their transparent conductive thin films, J. Colloid Interface Sci., 383 (2012) 36–42.
[63] G. Boczkaj, A. Fernandes, Wastewater treatment by means of advanced oxidation processes at basic pH conditions: a review, Chem. Eng. J., 320 (2017) 608–633.
[64] S. Zhang, G. Huihui, X. Xuetao, C. Ruya, Y. Hongcen, X. Xijin, L. Jiaxing, MOF-derived CoN/NC@SiO_2 yolk-shell nanoreactor with dual active sites for highly efficient catalytic advanced oxidation processes, Chem. Eng. J., 381 (2020) 122670, doi: 10.1016/j.cej.2019.122670.
[65] F. Saadati, N. Keramati, M. Mehdipour Ghazi, Influence of parameters on the photocatalytic degradation of tetracycline in wastewater: a review, Crit. Rev. Env. Sci. Technol., 46 (2016) 757–782.
[66] G. Fan, Z. Xiaomei, L. Jing, P. Huiping, L. Hui, B. Minchen, H. Liang, Z. Jinjin, Rapid synthesis of Ag/AgCl@ZIF-8 as a highly efficient photocatalyst for degradation of acetaminophen under visible light, Chem. Eng. J., 351 (2018) 782–790.
[67] Y. Boyjoo, A. Ming, P. Vishnu, Photocatalytic treatment of shower water using a pilot scale reactor, Int. J. Photoenergy, 2012 (2012) 578916, doi: 10.1155/2012/578916.
[68] T.E. Agustina, H.M. Ang, V.K. Pareek, Treatment of winery wastewater using a photocatalytic/photolytic reactor, Chem. Eng. J., 135 (2008) 151–156.
[69] E.E. Sann, P. Yong, G. Zhongfeng, Z. Shenshan, X. Fan, Highly hydrophobic ZIF-8 particles and application for oil-water separation, Sep. Purif. Technol., 206 (2018) 186–191.
[70] S. Jalali, M.R. Rahimi, K. Dashtian, M. Ghaedi, S. Mosleh, One step integration of plasmonic Ag_2CrO_4/Ag/AgCl into HKUST-1-MOF as novel visible-light driven photocatalyst for highly efficient degradation of mixture dyes pollutants: its photocatalytic mechanism and modeling, Polyhedron, 166 (2019) 217–225.
[71] S. Payra, C. Swapn, B. Yamini, C. Chanchal, G. Balaram, R. Sounak, Probing the photo-and electro-catalytic degradation mechanism of methylene blue dye over ZIF-derived ZnO, J. Hazard. Mater., 373 (2019) 377–388.
[72] C.H. Wu, C. Jia-Ming, Kinetics of photocatalytic decomposition of methylene blue, Ind. Eng. Chem. Res., 45 (2006) 6450–6457.
[73] N. Serpone, M.A. Yurii, K.R. Vladimir, V.E. Alexei, H. Satoshi, Light-driven advanced oxidation processes in the disposal of emerging pharmaceutical contaminants in aqueous media: a brief review, Curr. Opin. Green Sustainable Chem., 6 (2017) 18–33.
[74] A. Nezamzadeh-Ejhieh, M. Karimi-Shamsabadi, Comparison of photocatalytic efficiency of supported CuO onto micro and nano particles of zeolite X in photodecolorization of methylene blue and methyl orange aqueous mixture, Appl. Catal., A, 477 (2014) 83–92.